ACS APPLIED MATERIALS & INTERFACES

Research Article

www.acsami.org

Polycationic Macrocyclic Scaffolds as Potential Non-Viral Vectors of DNA: A Multidisciplinary Study

Ana L. Barrán-Berdón,[†] Belén Yélamos,[‡] Luis García-Río,[⊥] Òscar Domènech,[§] Emilio Aicart,[†] and Elena Junquera*[,†]

[†]Grupo de Química Coloidal y Supramolecular, Departamento de Química Física I, and [‡]Departamento de Bioquímica y Biología Molecular I, Facultad de Ciencias Químicas, Universidad Complutense de Madrid, 28040 Madrid, Spain

[⊥]Departamento de Química Física, Centro de Investigación en Química Biológica y Materiales Moleculares, Universidad de Santiago de Compostela, 15782 Santiago de Compostela, Spain

[§]Departamento de Fisicoquímica, Facultat de Farmàcia, Universitat de Barcelona, 08028 Barcelona, Spain

ABSTRACT: The potential of lipoplexes constituted by the DNA pEGFP-C3 (encoding green fluorescent protein), polycationic calixarene-based macrocyclic vector (CxCL) with a lipidic matrix (herein named TMAC4), and zwitterionic lipid 1,2-dioleoyl-*sn*-glycero-3-phosphatidylethanolamine (DOPE) as nontoxic DNA vectors has been analyzed from both biophysical and biochemical perspectives. For that purpose, several experimental methods, such as zeta potential (PALS methodology), agarose gel electrophoresis, small-angle X-ray scattering (SAXS), transmission electronic cryo-microscopy (cryo-TEM), atomic force microscopy (AFM), fluorescence microscopy, and cytotoxicity assays have been used. The electrochemical study shows that TMAC4 has 100% of its nominal charge available, whereas pDNA presents an effective negative charge that is only 10% that of its nominal one. PALS studies indicate the presence of three populations of nanoaggregates in TMAC4/DOPE lipid mixtures, with sizes of approximately 100, 17, and 6 nm, compatible with liposomes, oblate micelles, and spherical micelles, respectively, the first two also being detected by cryo-TEM. However, in the presence of pDNA, this mixture is organized in L_α multilamellar structures at all compositions. In fact, cryo-TEM micrographs show two types of multilamellar aggregation patterns: cluster-type at low and moderate CxCL molar fractions in the TMAC4/DOPE lipid mixture (α = 0.2 and 0.5), and fingerprint-type (FP), which are only present at low CxCL molar fraction (α = 0.2). This structural scenario has also been observed in SAXS diffractograms, including the coexistence of two different phases when DOPE dominates in the mixture. AFM experiments at α = 0.2 provide evidence that pDNA makes the lipid bilayer more deformable, thus promoting a potential enhancement in the capability of penetrating the cells. In fact, the best transfection perfomances of these TMAC4/DOPE-pDNA lipoplexes have been obtained at low CxCL molar fractions (α = 0.2) and a moderate-to-high effective charge ratio (ρ_{eff} = 20). Presumably, the coexistence of two lamellar phases is responsible for the better TE performance at low α.

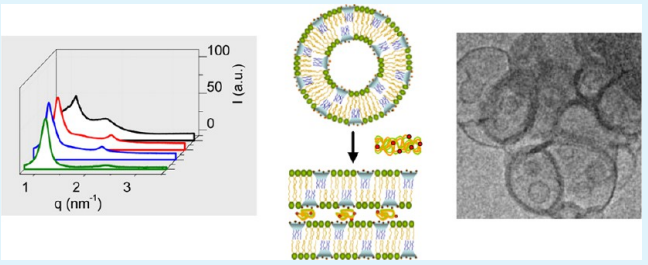

KEYWORDS: *macrocyclic gene vector, effective charges, effective charge ratios, calixarene-based vector, SAXS, AFM, zeta potential, transfection efficiency, cryo-TEM, multilamellar structures*

INTRODUCTION

One of the major challenges in gene therapy is to find safe and efficient gene carries. Much effort has been dedicated in the past decade to broadening the range of compounds capable of compacting, protecting, transporting, and delivering nucleic acids into the cell where the complex biological cell machinery will be in charge of expressing the proper proteins.[1−8] This string of actions is known as cell transfection, and the main aim of any group working in this field to carry on this complex process with the highest efficiency conjugated with the lowest danger (toxicity) to the cells, which must keep their integrity and remain viable for growth after transfection. In this respect, nonviral vectors present several advantages with respect to viral ones, as they can compact higher amounts of DNA, their production is cheaper, and they generally do not trigger an immune response.[2,3,9−15] However, their transfection efficiency and their cytotoxicity levels are areas that still require improvement. The most widely used nonviral vectors are cationic lipids (CLs),[2−4,13,16−23] presumably because of their significant similarity with the cell membrane and good levels of transfection; however, they also have several inconveniences, such as moderate-to-high cytotoxicity, nonspecific interactions with plasma proteins, and poor structural control of the complexes formed with DNA. In this regard, the synthesis of new compounds in the area of supramolecular chemistry has opened new possibilities to the design of chemical agents able

Received: April 14, 2015
Accepted: June 11, 2015
Published: June 11, 2015

DOI: 10.1021/acsami.5b03231
ACS Appl. Mater. Interfaces 2015, 7, 14404−14414

Scheme 1. Molecular Structures of (a) TMAC4 and (b) DOPE[a]

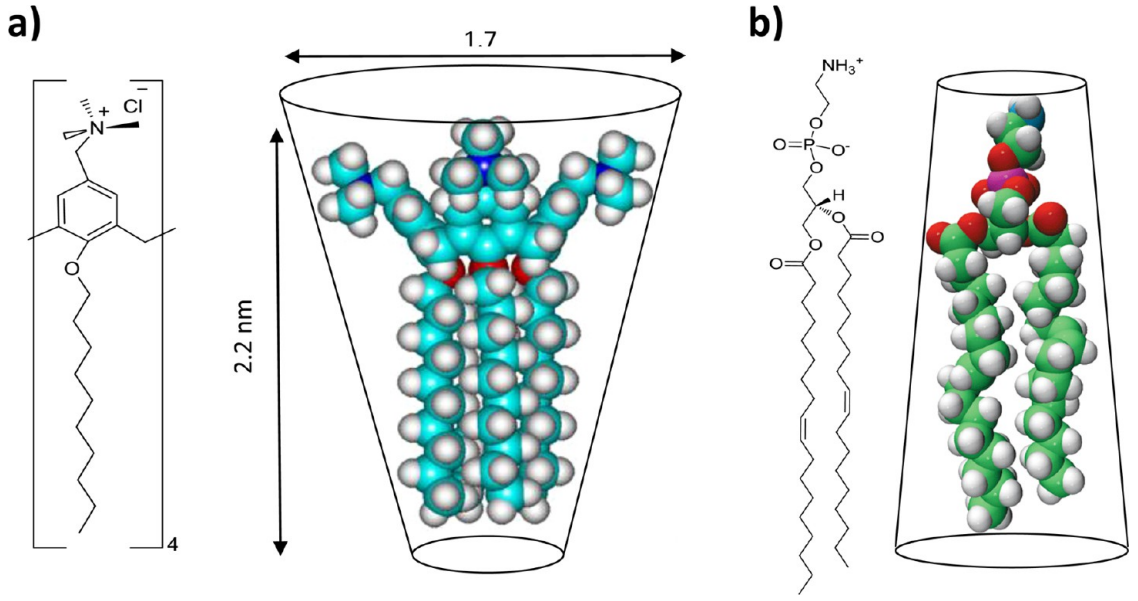

[a]CPK model of TMAC4 has been obtained with an MM-AMBER calculation, whereas that of DOPE has been taken from Avanti Polar Lipids.

to control their assembly with DNA by forming better defined and stable nanostructures, even in biological media.[24,25] A large number of gene vectors based on supramolecular building blocks have recently been proposed, one of the most important groups being macrocyclic molecules, such as cyclodextrins, fullerenes, calixarenes, and pilararenes.[24−32] Most of these molecules are characterized by a well-defined 3D topology, stable shapes, and an interesting facial amphiphilicity[24,33] that allows them to be functionalized on one face with adequate cationic groups that yield the necessary positive charge to act as DNA carriers, and, on the other face, with lipid-type chains that permit them to self-aggregate into well-defined aggregation patterns. In particular, calixarenes are macrocycles formed via a phenol-formaldehyde condensation and present a cuplike shape with a central hydrophobic cavity and an upper and lower rim that allows efficient region-selective chemistry, as described above.[34] For this reason, they are versatile macrocyclic compounds (CxCL) that combine the properties of both macrocyclic hosts and self-organizing systems, such as micelles and liposomes.[35] In addition, their relatively easy synthesis and their low toxicity levels make them really promising vectors in gene delivery applications. Conversely, it is known that zwitterionic lipids, such as 1,2-dioleoyl-*sn*-glycero-3-phosphoethanolamine (DOPE), play an important role in transfection processes because they increase the fusogenic properties of the vector and reduce the cytotoxicity of the complex. Several physicochemical and biological studies have been reported on a variety of calixarene-based vectors,[29−31,33,36−40] either mixed with helper lipids (as DOPE) or alone, and show that these macrocycles may efficiently compact DNA and are able to introduce biopolymers into cells through a subsequent transfection event. It is remarkable that none of these reported studies work with effective charges of both components of the lipoplex, the nanovector, and the plasmid, this fact being of special relevance given that it has been demonstrated that effective available charges (either positive from the vector or negative from the plasmid) are not always equivalent to their nominal ones.[23,41−43] Accordingly, more biophysical and biochemical characterizations are necessary to find an adequate correlation between physicochemical properties of the complexes formed (mostly electrochemical and structural characteristics) and their biological performances (transfection efficiency and cell viability) in what is called a structure−activity relationship (SAR). In this respect, this work reports a complete biophysical and biological study of the outcomes of a nonviral DNA vector of a mixed system consisting of DOPE and a polycationic calixarene-based lipid vector CxCL (TMAC4) with four trimethylammonium cationic groups on the upper ring of the macrocycle and four 10C chains on the lower ring. Scheme 1 shows the structure of both molecules. A series of high precision experimental techniques (including electrophoretic mobility-zeta potential, agarose gel electrophoresis, SAXS, cryo-TEM, and AFM) have been used to evaluate the electrochemical and structural characteristics of these nanoaggregates in the absence and presence of plasmid DNA, and with this information in mind, their capacity to transfect living human cancer cells in a safe way has also been verified by means of fluorescence microscopy and MTT assays.

EXPERIMENTAL SECTION

Materials. pEGFP-C3 plasmid DNA (pDNA) was extracted from competent *Escherichia coli* bacteria previously transformed with pEGFP-C3 with the extraction being carried out using a GenElute HP Select plasmid Gigaprep Kit (Sigma-Aldrich) following a previously described protocol.[42,44] Sodium salt of calf thymus DNA (ctDNA), provided by Sigma-Aldrich, was used as linear DNA to determine the lipid charge (q^{+}_{CxCL}) of the cationic vector. The zwitterionic lipid 1,2-dioleoyl-*sn*-glycero-3-phosphatidylethanolamine (DOPE) was purchased from Avanti Polar Lipids and has no charge at a physiological pH of 7.4. The polycationic calixarene-based lipidic vector CxCL is 5,11,17,23-tetrakis(trimethylammonio)-25,26,27,28-tetra-*n*-decyloxy calix[4]arene tetrachloride, referred to in this work as TMAC4; it was synthesized as described in the literature,[45] although the step for the chloromethylation was performed using a slightly modified literature procedure.[46] ^{1}H-NMR (300 MHz, DMSO-d_6): δ 6.88 (s, 8H, ArH), 4.48 (s, 8H, Ar-CH_2-N), 4.37 (d, 4H, Ar-CH_2-Ar), 3.89(t, 8H, Ar-O-CH_2), 3.32(d, 4H, Ar-CH_2-Ar), 2.94 (s, 36H,

DOI: 10.1021/acsami.5b03231
ACS Appl. Mater. Interfaces 2015, 7, 14404−14414

$N(CH_3)_3$), 1.88 (m,8H, -CH_2-CH_2-O-Ar), 1.32 (m, 56H, alkyl-CH_2), 0.85 (t, 12H, CH_3-CH_2-).

Preparation of Lipoplexes. Dry films of the mixture formed by the CxCL vector TMAC4 and the neutral helper lipid DOPE were prepared following a procedure fully described by our group previously.[42] Briefly, appropriate amounts of both components were dissolved in chloroform to obtain the desired CxCL molar fraction $\alpha = n_{CxCL}/(n_{CxCL} + n_{DOPE})$, where n_{CxCL} and n_{DOPE} are the moles of CxCL and DOPE, respectively, in the TMAC4/DOPE lipid mixtures, and afterwards, chloroform was removed under high vacuum to yield a dry lipid film. This dry film was subsequently hydrated with HEPES buffer (40 mM, pH = 7.4) and sequentially extruded according to a procedure also previously described.[47] Finally, equal volumes of pDNA and cationic vector suspensions were mixed to yield the desired lipoplex composition, which can be expressed either in terms of the mass ratio (m_{GV}/m_{DNA}) between total mass of the gene vector $m_{GV} = (m_{CxCL} + m_{DOPE})$ to plasmid DNA (m_{DNA}) or as the effective charge ratio (ρ_{eff}) between the CxCL and pDNA charges. pDNA concentrations were optimized to fit the optimum conditions for each experimental technique as follows: 0.05 mg/mL for zeta potential, 1 mg/mL for cryo-TEM, 200 μg/capillary for SAXS, 200 ng/well for gel electrophoresis, 0.05 and 0.5 mg/mL for AFM, 4 μg/mL each for the TE determination and fluorescence microscopy, and 1 μg/mL for the cell viability assays.

Characterization of Lipoplexes. Size and zeta potential measurements were run at 25 °C with a Phase Analysis Light Scattering technique (Zeta PALS, Brookhaven Instrum. Corp., USA).[42,43] Each electrophoretic mobility datum is taken as an average over 50 independent measurements. Zeta potentials for the lipoplexes were measured at different CxCL molar fractions (α) of the lipid mixture and at several m_{GV}/m_{DNA} ratios of the lipoplexes.

Small-angle X-ray scattering (SAXS) experiments were carried out on the beamline NCD11 at ALBA Synchrotron Barcelona (Spain). The energy of the incident beam was 12.6 keV (λ = 0.995 Å). The machine was run in multibunch mode with a filling pattern consisting of 10 trains, 64 ns long, and a gap of 24 ns between the trains. Samples were placed in sealed glass capillaries. The scattered X-ray diffraction pattern was detected on a CCD detector Quantum 210r, converted to one-dimensional scattering by radial averaging, and represented as a function of the momentum transfer vector. SAXS experiments were run at each α and at several effective charge ratios (ρ_{eff}) of the lipoplexes.[42]

Cryo-TEM experiments were run for TMAC4/DOPE mixtures in the absence and presence of pDNA, following standard procedures.[48,49] In these experiments, perforated Quantifoil R1.2/1.3 (1.2 μm hole diameter) on a 400-mesh copper grid were used. Images were obtained using a Jeol JEM 2011 cryo-electron microscope operated at 200 kV under low-dose conditions and using different degrees of defocus (500−700 nm) to obtain an adequate phase contrast.[50] Images were recorded on a Gatan 794 Multiscan digital camera. These CCD images were processed and analyzed with a Digital Micrograph.

Liquid AFM imaging was performed at room temperature using a Multimode Microscope controlled by Nanoscope V electronics (Bruker, AXS Corporation, Madison, WI). Sample images were acquired in contact mode using MSNL-10 V-shaped Si_3N_4 cantilevers (Bruker AFM Probes, Camarillo, CA) with a nominal spring constant of 0.03 N m^{-1}. The scan velocity was 3 Hz, and feedback parameters were optimized to apply the minimum vertical force. Supported lipid bilayers (SLBs) were spread on mica surfaces by vesicle fusion. Briefly, 60 μL of 250 μM TMAC4/DOPE liposomes in 40 mM HEPES buffer, pH 7.40, were deposited onto freshly cleaved mica disks. Samples were incubated at 37 °C for 30 min in an oven using a water reservoir to prevent evaporation of the water from the sample. After this period, samples were washed with buffer to eliminate the nondeposited lipids. Before scanning, it was necessary to drift equilibrate and thermally stabilize the cantilever in the presence of buffer for no less than 30 min. All images were processed using NanoScope Analysis Software (Bruker AXS Corporation, Santa Barbara, CA).

Biochemical Outcomes of Lipoplexes. Once TMAC4/DOPE lipid mixtures were prepared in the absence of serum (−FBS), the transfection of pEGFP-C3 plasmid DNA into HEK293T cells (human embryo kidney transformed cancer) using these lipid mixtures was performed in the presence of serum (+FBS) at several charge ratios. Each sample was prepared in duplicate, and experiments were independently repeated twice for each composition. Transfection efficiency (TE) was evaluated by means of fluorescence microscopy. Control experiments were performed using the commercial transfection reagent Lipofectamine2000* (Lipo2000*).[51]

The cytotoxicity and cell viability of each lipid formulation toward HEK293T cells was determined using the 3-(4,5-dimethylthiazole-2-yl)-2,5-diphenyl tetrazolium bromide reduction method (MTT assay) following a literature procedure.[52,53] Lipoplexes were prepared using 50 ng of pDNA per sample with the appropriate amount of TMAC4/DOPE mixtures to obtain the desired α and ρ_{eff} ratios. As fully detailed previously,[51] the percent cell viability was spectrophotometrically determined with an ELISA reader.

RESULTS AND DISCUSSION

It is well-known that plasmids are mostly in supercoiled conformations when they are at physiological conditions of pH and ionic strength with this fact having a notorious effect on their effective charges. In fact, we have previously demonstrated[42,43,54] that when they are compacted by cationic lipid vectors, their effective charges are only 10−25% their nominal ones. This feature has quite important implications for the cytotoxicity of the gene vector, and in turn, on their transfection effectiveness. For this reason, we believe that the first step of any biophysical study of pDNA compaction and transfection must necessarily rely on an electrochemical study aimed to determine the effective charges of both components of the lipoplex system (i.e., cationic gene vector and pDNA). In this respect, we have developed and published a procedure to fulfill this objective[42−44] based on a two-step protocol that uses the experimental zeta potential measurements as a function of lipoplex composition to determine, (i) in the first step, the effective charge of the cationic vector by characterizing the lipoplexes formed by this vector and double stranded linear DNA (ctDNA, with a well established charge of −2/bp), and (ii) in the second step, the effective charge of the pDNA by characterizing the lipoplex formed by the cationic vector of already known charge (step i) and the pDNA. Figure 1 shows the zeta potential measurements relative to lipoplex composition for both types of lipoplexes at different CxCL molar compositions of the TMAC4/DOPE mixtures. Lipoplex

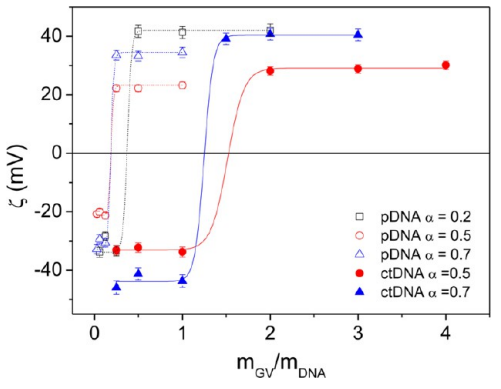

Figure 1. Plots of zeta potential against the lipoplex composition (m_{GV}/m_{DNA}) of TMAC4/DOPE-DNA lipoplexes, ctDNA (solid symbols), and pDNA (open symbols) for several CxCL molar fraction of the TMAC4/DOPE lipid mixture at α = 0.2 (squares), α = 0.5 (circles), and α = 0.7 (triangles).

DOI: 10.1021/acsami.5b03231
ACS Appl. Mater. Interfaces 2015, 7, 14404−14414

compositions are expressed in terms of mass ratios, m_{GV}/m_{DNA}, with m_{GV} being the total mass of the cationic gene vector ($m_{GV} = m_{CxCL} + m_{DOPE}$) (i.e., the sum of the mass of the calixarene-based cationic lipid vector, m_{CxCL}, and the mass of the neutral zwitterionic lipid DOPE, m_{DOPE}) and the total mass of the biopolymer (m_{DNA}). As is typically observed, lipoplexes constituted by plasmids reach the electroneutral composition at lower values than those formed by linear DNA for a given DNA concentration.

From the data in Figure 1 and the protocol commented on above (and fully described in ref 44), we have found that the calixarene-based cationic lipid vector used herein (TMAC4) has an effective charge of +4 (within an experimental uncertainty of <10%), whereas the pEGFP-C3 plasmid DNA only yields ∼10% of its nominal charge with an average effective charge of (−0.25 ± 0.03) /bp. This behavior is consistent with that previously found for other cationic lipid vectors already studied in our lab[23,41−44,54] (i.e., the cationic lipid vectors normally yield their total nominal positive charges within a range of 10% of uncertainty, whereas plasmids usually retain an important percentage of its cationic Na^+ counterions, yielding an effective negative charge that is much less negative than that of its nominal one). This behavior has very important consequences on the potential of these systems as safer and effective gene vectors because as long as the charge of the DNA is less negative the necessities of the cationic vector are also fewer, thus decreasing the cytotoxicity of the vector.

Once these effective charges are known, lipoplex compositions may and have to be expressed in terms of the effective charge ratios, defined as

$$\rho_{eff} = \frac{n^+}{n^-} = \frac{(q^+_{CxCL} m_{CxCL})/M_{CxCL}}{(q^-_{pDNA} m_{pDNA})/M_{pDNA}}$$

where n^+ and n^- are the number of moles of positive and negative effective charges coming from the cationic vector and pDNA, respectively, q^+_{CxCL} and M_{CxCL} are the effective charge and the molar mass of the cationic calixarene-based vector, respectively, and q^-_{pDNA} and M_{pDNA} are the effective charge and the average molar mass of pDNA per base pair (/bp), respectively. Notice that, for this particular system, considering the effective charges obtained and those described above, the relation between effective and nominal charges ratios is $\rho_{eff} = 8\,\rho_{nom.}$

The compaction level of pDNA by TMAC4/DOPE formulations may be also evaluated by means of agarose gel electrophoresis experiments. These studies (see Figure 2) were performed at α = 0.20 (lanes 2−4), 0.5 (lanes 5−7), 0.7 (lanes 8−10), and 1 (lanes 11−13), each of them at effective charge ratios (ρ_{eff}) of 2, 5, and 20, together with those for uncomplexed pDNA (lane 1) as a positive control. Results reported in Figure 2 reveal that pDNA is efficiently compacted by cationic mixed TMAC4/DOPE liposomes because the fluorescent bands disappear across the gel lanes as long as either ρ_{eff} and/or α increase. Note that at α = 0.2, pDNA is not totally compacted (i.e., fluorescence emission of the probe Gel Red can be seen along the gel lane) until ρ_{eff} values are >5, whereas at α = 0.7, no fluorescence in the gel lane is already detected at ρ_{eff} = 2. This behavior is consistent with that reported by Rodik et al.[38] for a similar calixarene/pDNA lipoplex. It is remarkable that, in their study, pDNA seems to be compacted by the calixarene at very low charge ratios of ∼0.5; however, it must be noted that the nominal charge of pDNA (−2/bp) is used instead of the effective charge, which in the present case is approximately eight times less negative (−0.25/bp). Accordingly, the charge ratio for which Rodik et al. found the pDNA compaction should be ∼1 order of magnitude higher than that reported, which would be totally consistent with our results. In any case, these results indicate that (i) the higher the content of cationic vector in the mixture (increase in either α or ρ_{eff}), the more efficient the compaction of pDNA, in agreement with the zeta potential results; moreover, (ii) despite being positively charged (ρ_{eff} > 1), a certain percentage of pDNA is still uncompacted because, although with much lower intensities, fluorescence bands are still observable.

The self-aggregation pattern, structure, and size of the gene vector are known to play an important role on the pDNA compaction process, and for that reason, structural information is always very welcome. It is documented that calixarene-based lipidic vectors form micelles in aqueous media,[31,38,45] but there is not anything reported regarding the self-aggregation pattern of mixed systems such as that described in this work, in which the macrocyclic-type vector is mixed with a zwitterionic lipid (DOPE) widely used as a neutral lipid (at physiological pH conditions) with a well-known fusogenic character. However, it is a presumably interesting information because the same study that reports the micelle-type aggregates for a CxCL similar to the one presented here[38] also concludes that the presence of DOPE in the mixture improves the transfection outcome of the cationic vector. For this reason, the sizes of the TMAC4/DOPE formulations have been determined with the PALS technique at α = 0.2, 0.5, and 0.7. Figure 3 shows the size distributions obtained at α = 0.5 as an example. As can be seen in Figure 3, the TMAC4/DOPE mixtures contain a majority population of

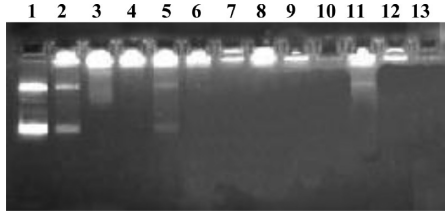

Figure 2. Gel electrophoresis results for TMAC4/DOPE-pDNA lipoplexes at several CxCL molar fractions of the TMAC4/DOPE lipid mixture: α = 0.2 (lines 2−4), α = 0.5 (lines 5−7), α = 0.7 (lines 8−10), and α = 1.0 (lines 11−13) at charge ratios of ρ_{eff} = 2 (2, 5, 8, and 11), ρ_{eff} = 5 (3, 6, 9, and 12), and ρ_{eff} = 20 (4, 7, 8, and 13); line 1 shows the results of pDNA as a control.

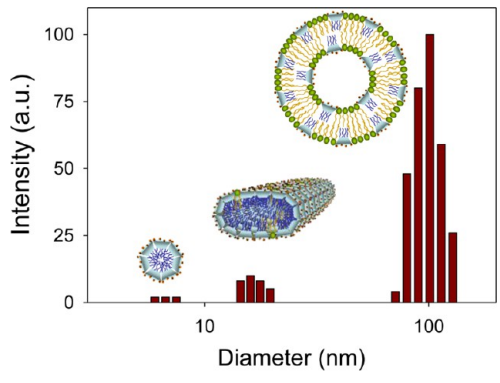

Figure 3. Hydrodynamic diameter of TMAC4/DOPE nanoaggregates at α = 0.5 obtained with the PALS technique.

DOI: 10.1021/acsami.5b03231
ACS Appl. Mater. Interfaces 2015, 7, 14404−14414

self-aggregates with average diameters of ∼100 nm, although there are two minority populations of self-aggregates with average sizes of approximately 17 and 6 nm. These sizes are compatible with mixed spherical liposomes, oblate micelles, and spherical micelles, respectively, as shown in the 2D drawings included in Figure 3. Table 1 reports the averaged diameters of these aggregates at all of the studied compositions. It is noticeable that both micelle populations disappear at low α, where DOPE is the predominant component, and they become more relevant when the CxCL content increases (i.e., α tends to 1), in agreement with the literature.[33]

Table 1. Hydrodynamic Diameters of the TMAC4/DOPE Nanoaggregates Determined at Different CxCL Molar Fractions of the TMAC4/DOPE Lipid Mixture (α) with the Zeta PALS Technique along with the Percentages of Each Nanoaggregate Population

α	ϕ_1 (nm)	%	ϕ_2 (nm)	%	ϕ_3 (nm)	%
0.2					120	100
0.5	6	2	17	6	100	92
0.7	7	5	20−25	32	150−160	63

Cryo-TEM experiments were run in this work as well for TMAC4/DOPE mixtures at α = 0.5. Figure 4 shows three cryo-TEM micrographs selected among those obtained for this system. It is remarkable that, when mixed with DOPE, most micrographs indicate that the calixarene-based cationic lipid TMAC4 aggregates form essentially in unilamellar and spherical liposomes (panels a and b) with a diameter of ∼(90 ± 8) nm averaged over the structures found in all of the micrographs (not only those shown in Figure 4). This size is in very good agreement with the PALS results, mostly considering that the size information given by the PALS technique is based on hydrodynamic data. However, some micrographs (see panel c in Figure 4) also show a population of small aggregates with sizes of ∼20 nm, which are compatible with the presence of oblate micelles, such as those found by PALS. The right panels in Figure 4 show 2D drawings of these two types of mixed nanoaggregates: liposomes and oblate micelles. However, the spherical micelles found with the PALS technique (average diameters of ∼6−7 nm) are not detected by cryo-TEM. All of these sizes are consistent with the extrusion protocol used,[47] which is based on a sequential procedure that ends with a final pass of the mixed liposome solution through a polycarbonate membrane with pores of 100 nm in diameter.

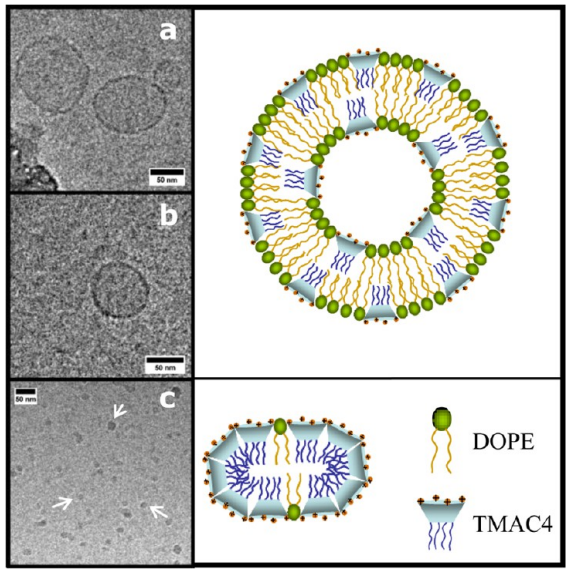

Figure 4. (left) A selection of cryo-TEM micrographs showing a general view of the TMAC4/DOPE mixed nanoaggregates at α = 0.5 with (a, b) mixed liposomes and (c) disk-like (oblate) micelles (see arrows). (right) Schematic 2D drawings of liposome and disk-like (oblate) micelles.

With the aim of gaining more insight into the structural and morphological aspects of these nanoaggregates when pDNA is present, concentrated samples of TMAC4/DOPE-pDNA lipoplexes were analyzed by means of both SAXS and cryo-TEM at different effective charge ratios (ρ_{eff}) at which lipoplexes are potentially active as gene therapy vectors (ρ_{eff} > 1) and covering a wide range of CxCL molar fractions of the lipid mixture (α). Figure 5 shows SAXS diffractograms (intensity vs q factor) at ρ_{eff} = 1.5, 2, and 4 for several CxCL molar fractions of the TMAC4/DOPE lipid mixture. The

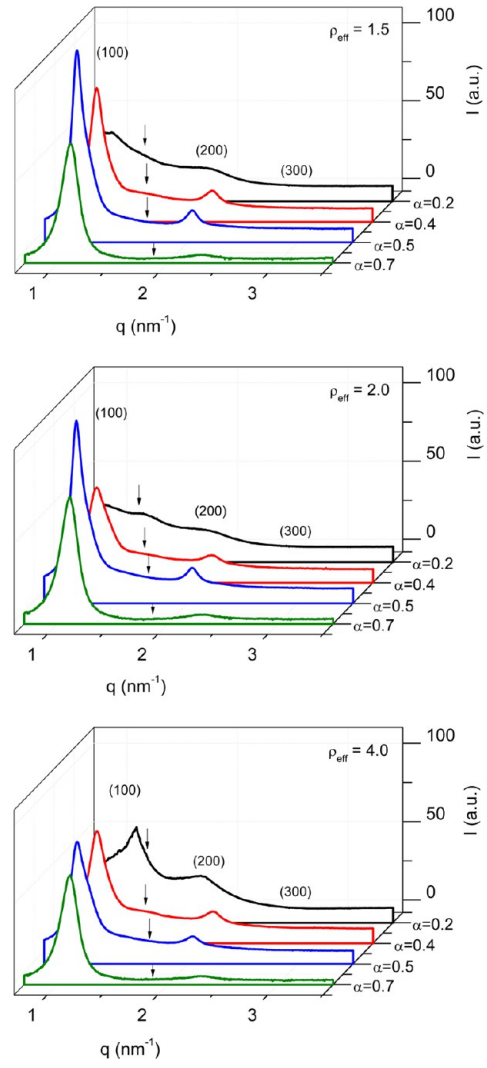

Figure 5. SAXS diffractograms of TMAC4/DOPE-pDNA lipoplexes at several charge ratios ρ_{eff} = 1.5, 2.0 and 4.0, and for each charge ratio, at various CxCL molar fractions: α = 0.2, black lines; 0.4, red lines; 0.5, blue lines; and 0.7, green lines. Arrows indicate the pDNA−pDNA correlation peak.

DOI: 10.1021/acsami.5b03231
ACS Appl. Mater. Interfaces 2015, 7, 14404−14414

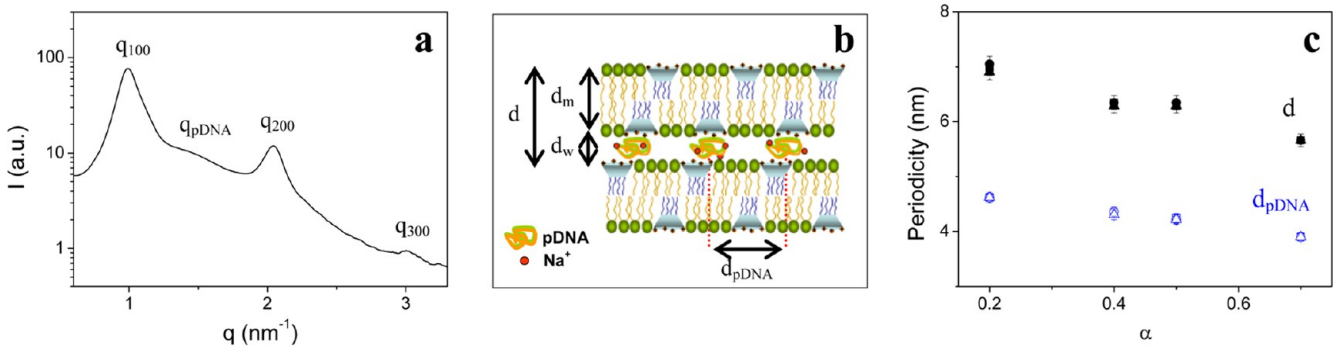

Figure 6. (a) SAXS diffractograms for TMAC4/DOPE-pDNA lipoplexes at $\alpha = 0.2$ and $\rho_{eff} = 1.5$ in logarithmic scale; (b) schematic drawings of 2D views of a lamellar L_α phase, showing the characteristic distances; (c) plots of periodic distance of the lamellar structure (d) and the pDNA−pDNA correlation (d_{pDNA}) for TMAC4/DOPE-pDNA lipoplexes versus CxCL molar fraction (α) at several charge ratios (ρ_{eff}). Square, $\rho_{eff} = 1.5$; circle, $\rho_{eff} = 2.0$; and triangle, $\rho_{eff} = 4$.

Miller indexes, shown over the Bragg peaks in the diffractograms, indicate that TMAC4/DOPE and pDNA mixtures are structured in terms of typical multilamellar phases (L_α), where pDNA supercoils are stacked and compacted within the aqueous monolayer, which is located between alternating bilayers constituted by the mixture of the CxCL vector and DOPE in a sandwich-fashion pattern. This L_α phase is characterized by two distances: (i) the interlayer distance (d) related to the q factor of the first peak ($d = 2\pi/q_{100}$), which can be expressed as the sum of the thicknesses of the lipidic bilayer (d_m) and the pDNA aqueous layer (d_w), and (ii) the separation between pDNA supercoils (i.e., pDNA−pDNA correlation) in this sandwiched aqueous monolayer, d_{pDNA}, which can be obtained from the q_{pDNA} factor of the Bragg broad peak not corresponding to the lamellar structure that appears in the middle of all of the diffractograms ($d_{pDNA} = 2\pi/q_{pDNA}$). In fact, panel a of Figure 6 tries to show more clearly (using a logarithmic scale) the unambiguous presence of this pDNA Bragg peak as well as those belonging to the L_α phase with very low intensities. Panel b of Figure 6 shows a 2D-drawing of this phase with these characteristic structural parameters shown. Both d and d_{pDNA} distances have been calculated and plotted versus α in panel c of Figure 6 for all of the ρ_{eff} studied. As can be noted, d decreases from 7 to 5.5 nm, as long as the percentage of the calixarene-based lipidic vector increases in the bilayer, mostly because a higher positive surface density charge may provoke an enhanced level of pDNA compaction, which in turn yields a decrease in d_w. Another factor could be that the hydrophobic region of TMAC4 is shorter than that of DOPE; accordingly, as long as α increases, the thickness of TMAC4/DOPE bilayer may experience a slight decrease. Likewise, the higher the cationic density charge of the bilayer surface (i.e., α increases), the shorter the distance between pDNA supercoils in the aqueous monolayer (d_{pDNA} decreases); in fact, as shown in the Figure 6, d_{pDNA} decreases from 4.5 to ∼4 nm, revealing a clear enhancement of the pDNA compaction level as long as the content of TMAC4 in the bilayer increases. These results are consistent with those previously reported for other CL/DOPE systems.[23,41,44]

Cryo-TEM experiments were also run on positively charged TMAC4/DOPE-pDNA lipoplexes for $\alpha = 0.2$ and 0.5. Figure 7 shows a selection of micrographs among those taken. As can be observed, two different compaction patterns can be distinguished: (i) clusters of nanostructures with a well-defined multilamellar profile (see panels a and b), and (ii) regions with a continuum arrangement of multilamellae following a typical

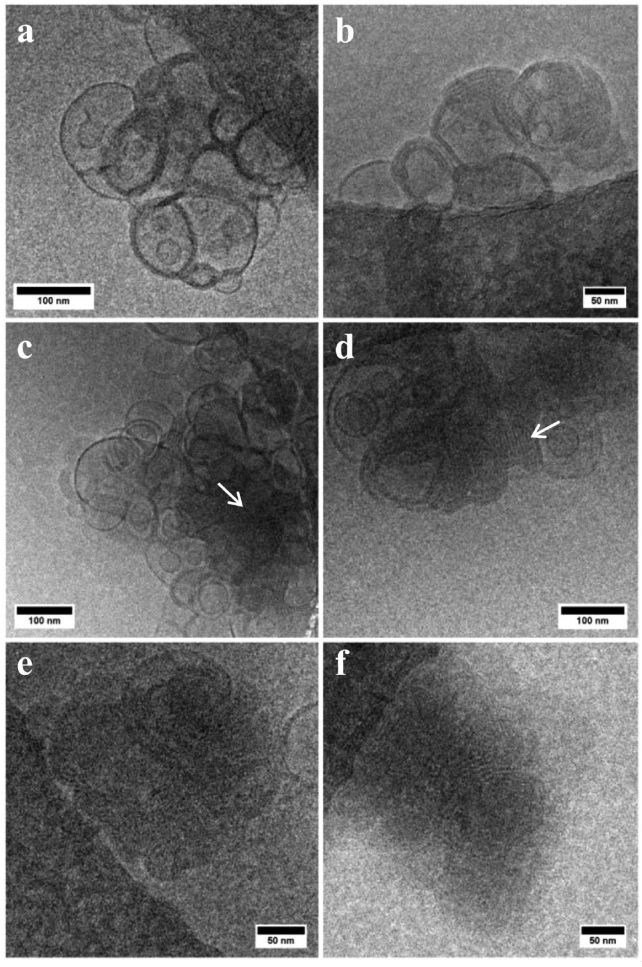

Figure 7. A selection of cryo-TEM micrograph showing a general view of the TMAC4/DOPE-pDNA lipoplex nanoaggregates at CxCL molar fractions of $\alpha = 0.2$ (a−d) y $\alpha = 0.5$ (e, f). White arrows point to FP domains coexisting with CT-type structures.

fingerprint pattern (panels e and f). Both scenarios have been found previously for other lipoplexes that we have studied.[23,41,44] The first, characterized by a series of cationic lipidic bilayers with pDNA sandwiched between them in what has been called clusterlike lipoplexes (CT-type nanoaggregates), is usually found in the DOPE-rich region (low values of α). It seems that when the content of DOPE is high, the lipoplexes

DOI: 10.1021/acsami.5b03231
ACS Appl. Mater. Interfaces 2015, 7, 14404−14414

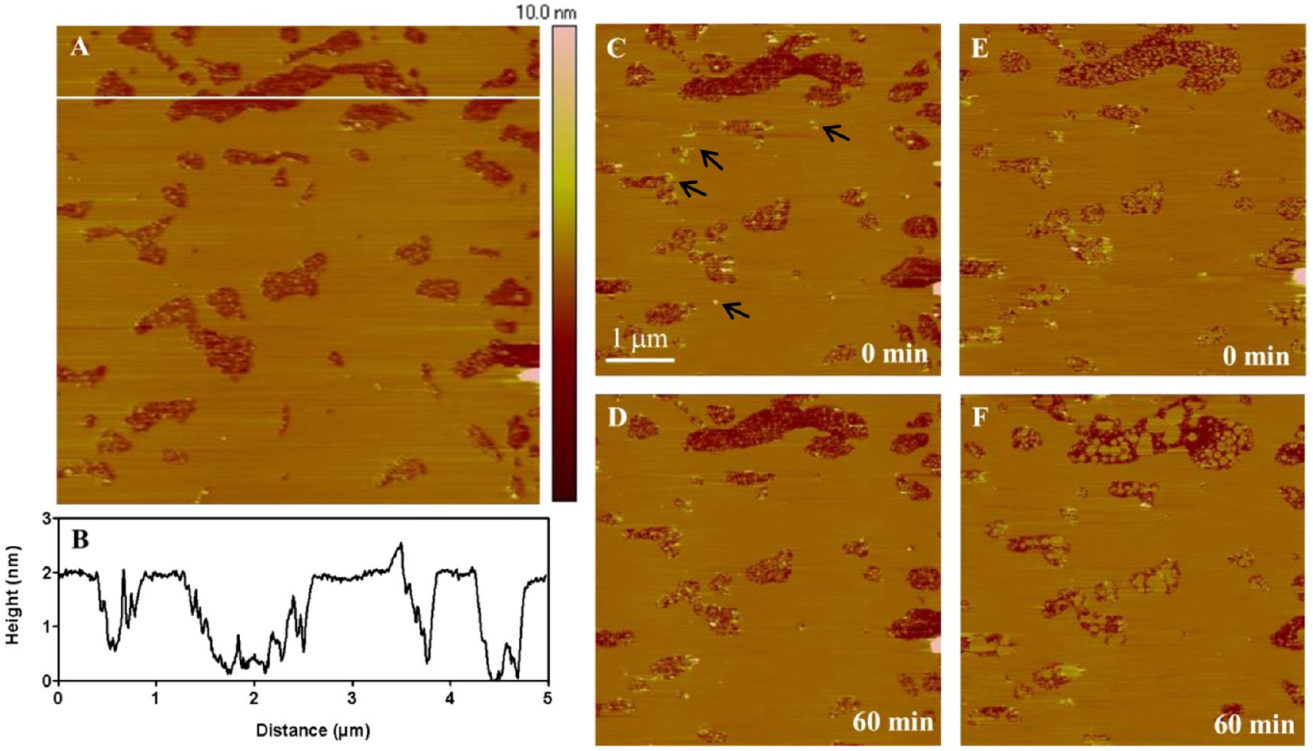

Figure 8. AFM images of TMAC4/DOPE (α = 0.2) in the absence (A, B) and presence (C–F) of pDNA. (A) Supported lipid bilayer control image, (B) height profile along white line in panel (A), (C and D) SLB after the injection of pDNA to a final concentration of 0.05 mg/mL (ρ_{eff} = 4), (E and F) SLB after the injection of pDNA to a final concentration of 0.5 mg/mL (ρ_{eff} = 0.4). Black arrows point to small pDNA aggregates.

tend to aggregate, leading to the formation of clusterlike nanostructures, where the lipidic bilayers, although deformed when sandwiching pDNA supercoils with the adjacent bilayers, essentially retain their morphologies. In fact, we can observe how the bilayers thicken and twist or even loop without disruption. The second scenario, usually found when DOPE content decreases, is characterized by a clear fingerprint compaction pattern, and for that reason, this kind of nanostructure has been called FP-type nanoaggregates. In contrast to the CT-type lipoplexes, liposomes tend to disrupt in FP-type, probably because liposome–pDNA interactions are clearly favored in this case. This fingerprint pattern, associated with multilamellar nanoaggregation, is also documented in the literature for lipoplexes of linear DNA and monovalent CLs.[55−59] Analyzing Figure 7, one can conclude that CT-type nanoaggregates are clearly found at α = 0.2 (panels a and b), whereas FP-type lipoplexes are essentially seen at α = 0.5 (panels e and f). However, coexisting with CT-type patterns at α = 0.2, one can observe regions of certain populations of FP-type lipoplexes (see arrows in panels c and d). This coexistence of phases, previously found for lipoplexes formed by gemini cationic lipids as well and potentially responsible for a synergistic effect on transfection,[41,42,44] would be consistent with the form adopted by the diffractograms found at α = 0.2 characterized by broad peaks of low intensity that are probably convoluted by more than one component. In any case, the average values obtained for the interlamellar distance of CT and FP-type multilamellar nanoaggregates indicate that, although the FP-type pattern shows much more lamellae than CT-type nanoaggregates, there is no appreciable difference on pDNA compaction among both multilamellar patterns.

It is noticeable that the inverse hexagonal phase H_{II}^{C}, characterized by inverse cylindrical micelles with the plasmid molecules allocated inside the cylinders and previously found in other CL/DOPE-pDNA lipoplexes at low α values,[44,60] has not been found in the present system. The reason may be that the Israelachvili packing parameter of TMAC4, clearly below 0.33 and thus typical of a lipid with a natural tendency to form micelles, is somehow "compensated" by the packing parameter of DOPE, which is clearly above 1 and thus typical of lipids that aggregate in the form of inverse phases (see Scheme 1). Consequently, the mixture TMAC4/DOPE tends to self-organize in the form of lamellar phases, as seen both in SAXS and cryo-TEM results, with a curvature that would depend on the content of DOPE in the mixture.

Undoubtedly, the interaction between pDNA and the lipidic membranes is another key factor in the transfection process. AFM is known to be one of the techniques of choice to visualize this interaction. Accordingly, AFM experiments have been run for TMAC4/DOPE samples in the absence and presence of pDNA at two concentrations and two incubation times (see Figure 8). Table 2 lists the values for the height, R_a, and covering percentage statistics from the AFM images in Figure 8. Panels A and B in Figures 8 show the AFM image of the SLB of a TMAC4/DOPE sample at α = 0.2 and the step

Table 2. Height, Roughness (R_a) and Covering Percentage Statistics from AFM Images in Figure 8

[DNA] (mg mL^{-1})	ρ_{eff}	incubation time (min)	height (nm)	R_a (nm)	coverage (%)
0		0	1.5 ± 0.2	0.07	84
0.05	4	0	2.0 ± 0.4	0.18	88
0.05	4	60	2.2 ± 0.4	0.13	87
0.5	0.4	0	2.8 ± 0.4	0.12	94
0.5	0.4	60	2.9 ± 0.3	0.11	93

DOI: 10.1021/acsami.5b03231
ACS Appl. Mater. Interfaces 2015, 7, 14404−14414

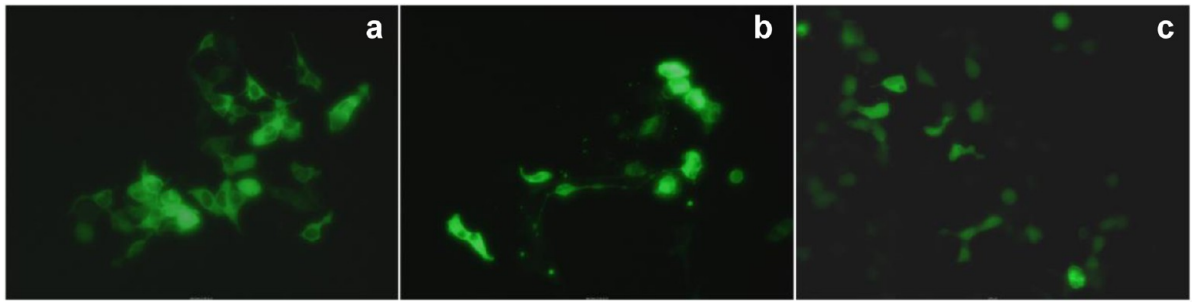

Figure 9. Representative images of fluorescence microscopy showing GFP expression in HEK293T cells transfected in the presence of serum (+FBS) with TMAC4/DOPE-pDNA lipoplexes at α = 0.2 for (a) ρ_{eff} = 20, (b) ρ_{eff} = 40, and (c) control Lipo2000*.

height profile along the white line, respectively. It is clearly seen that this SLB is a uniform flat surface with a roughness (R_a) mean value of 0.07 nm and high % coverage (~84%). Remarkably, the step height from the mica surface to the top of the SLB is (1.5 ± 0.2) nm, which is small for a lipid bilayer (less than the typical thickness of a half-bilayer), but already reported for DOPE-containing lipid bilayers.[61] Several reasons could account for this value: (i) DOPE is a phospholipid with a melting temperature of −16 °C, being in a fluid phase at room temperature and even moreso at 37 °C. This fact makes the SLB studied, which consists of 80% DOPE, notably fluid; the lipids have been tilted in the transduced layer, resulting in a decrease in the expected step height of the lipid layer. (ii) The mica surface (dark regions in Figure 8A) may be partially covered with lipids that are not arranged in a bilayer form, as can be observed from Figure 8B, where it is shown that the mica surface is not flat, which could disturb correct height measurements. Or, (iii) the AFM probe, upon contact with this SLB, could press and even deform the surface of the fluid TMAC4/DOPE bilayer, as has also been found for other SLBs formed from mixtures of DOPE and other lipids.[61]

Figure 8C shows the AFM image of the SLB surface of TMAC4/DOPE after the injection of pDNA to a final concentration of 0.05 mg/mL (ρ_{eff} = 4); as can be seen, many small aggregates (black arrows) appear on the SLB surface. The addition of the pDNA slightly increases both the R_a value, the covering of the lipid layer, and the SLB height (see Table 2), suggesting the adsorption of small particles, probably small pDNA aggregates. However, after 1 h of incubation (Figure 8D), those aggregates have decreased in number, either because they have been moved away during the scanning or because they disaggregate and extend onto the flat SLB surface. Furthermore, after this incubation time, the SLB becomes flatter (R_a value of 0.13 nm), and in some SLBs, extends to become slightly taller (step height ~2.2 nm), although the covering remains essentially unaffected. In any case, no individual extended pDNA molecules are observed under the experimental conditions.

To verify if the SLB modifications are induced by the pDNA molecules, we increased the pDNA concentration in the sample. Figure 8E shows an AFM image after the injection of pDNA to reach a concentration of 0.5 mg/mL (ρ_{eff} = 0.4); an increase in the SLB step height to 2.8 nm is observed with the R_a value being almost unchanged, increasing the coverage of the mica surface. A possible explanation for the increase in the step height together with a more covered surface is that individual pDNA molecules are being adsorbed in the SLB although they are not observed. Interestingly, after 1 h of incubation (Figure 8F), the small patches inside the different holes in the SLB fuse to form new, large structures with similar height and R_a values as the SLB. This fact is evidenced by the mobilization and rearrangement of lipids when pDNA is present in the system. In other words, pDNA molecules seem to facilitate the lipid reorganization even when lipids are adsorbed onto a solid surface, such as the mica surface. If this behavior is extrapolated to the TMAC4/DOPE lamellar phases observed in solution at α = 0.2, it can be concluded that the presence of pDNA turns the lipid bilayer into a more deformable one, thus enhancing their capability to penetrate the cells more easily.

The electrochemical and structural discussion included above must be completed with a biochemical evaluation of both the capacity of the polycationic macrocyclic vector to transfect pDNA into cells and its cytotoxicity. An optimum gene vector is one that presents the highest level of transfection efficiency conjugated with the lowest level of cytotoxicity (i.e., highest level of cell viability). Accordingly, transfection efficiencies (TE) of the lipoplexes studied herein were evaluated in HEK293T cells in the presence of serum using fluorescence microscopy experiments. The transfection studies were carried out at different CxCL molar fractions of the TMAC4/DOPE lipid mixture (α) each at different values of ρ_{eff}. Figure 9 shows the best TE results obtained (i.e., the fluorescence micrographs of HEK293T cells for the optimum formulations (α = 0.20, ρ_{eff} = 20 and 40) and Lipofectamine2000* as a positive control) in the presence of serum (+FBS). No significant levels of GFP expression were found at other liposome and lipoplex compositions. The observation of green images in the micrographs is indicative that efficient pDNA transfection to the nucleus of cells has occurred, thus promoting the expression of GFP. Accordingly, the fluorescence micrographs of Figure 9 reveal that TMAC4/DOPE formulations seem to be able to compact, protect, and transfect the green fluorescent protein encoding plasmid DNA pEGFP-C3 (pDNA) in HEK293T cells in the presence of serum with comparable efficiencies at the two ρ_{eff} values reported (20 and 40), although slightly better results can be inferred at ρ_{eff} = 20. Furthermore, comparing GFP expression levels of panels a and b with that shown in c (positive control), one can also conclude that any of the TMAC4/DOPE formulations seem to yield slightly better TE outcomes than the control Lipofectamine2000* (panel c), which is a commercial lipidic formulation consisting of a mixture of CLs (cationic lipids). These results are consistent with those reported in the literature by Rodik et al. for a similar system[38] at ρ_{nom} = 2.5 and 5. Notice that the electrochemical study reported herein has evidence that the effective negative charge of the pDNA used is −0.25/bp instead of the nominal charge of −2/bp normally found in the literature. This means that our values for ρ_{eff} = 20 and 40 are equivalent to those for

DOI: 10.1021/acsami.5b03231
ACS Appl. Mater. Interfaces 2015, 7, 14404−14414

ρ_{nom} = 2.5 and 5.[38] It is also remarkable that the best TE levels have been found at a low molar fraction (α = 0.20), where DOPE is the main component of the lipidic vector, and furthermore, where coexistence of two multilamellar phases (CT- and FP-type) has been observed. This evidence, the key roles of both DOPE and the coexistence of phases, has also previously been found for lipoplexes constituted by mixtures of different gemini cationic lipids (GCLs) and DOPE.[23,41,42,44] Additionally, it has also been interesting to find in this work from AFM experiments that, also at a low CxCL molar fraction, pDNA seems to favor a more deformable lipidic membrane, thus clearly promoting cell penetration and, in turn, enhancing the transfection efficiency (TE).

Finally, the cytotoxicity of the TMAC4/DOPE-pDNA lipoplexes studied herein was evaluated by means of MTT assays, which provide data on the percentage of cells that remain viable to grow and divide 48 h post transfection. MTT assays were performed on HEK293T at α = 0.20 and ρ_{eff} = 10, 20, 40, and 80 (see Figure 10) with Lipofectamine2000* being

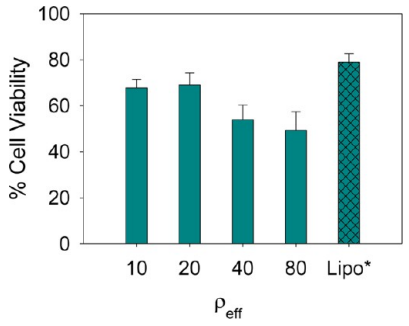

Figure 10. Cell viability of the HEK293T cell line transfected with TMAC4/DOPE-pDNA lipoplexes at α = 0.2 and several ρ_{eff}. Lipo* corresponds to results obtained with control Lipofectamine2000* in the presence of serum (+FBS).

used as a positive control. As seen in Figure 10, the viability of the HEK293T transfected cells in the presence of TMAC4/DOPE-pDNA lipoplexes is comparable in general terms to that measured in the presence of control Lipofectamine2000*. In fact, the best results have been found at α = 0.20 and ρ_{eff} = 10 and/or 20 with a percent cell viability of ~70% as the viability clearly decreases for higher values of ρ_{eff}. Combining this evidence with the fact that the best TE levels have been reached for ρ_{eff} = 20 and/or 40, one can conclude that a CxCL molar fraction of α = 0.20 and a charge ratio of ρ_{eff} = 20 for TMAC4/DOPE-pDNA lipoplexes, characterized by fluid membranes and the coexistence of two L_α phases with both CT and FP multilamellar patterns, are the parameters of choice in this system for a moderately efficient transfection process. Nonetheless, it must be noted that the transfection efficiencies of TMAC4/DOPE-pDNA lipoplexes are lower than those of some other GCL (gemini cationic lipid) formulations that we have previously reported,[23,41,42] and in any case, comparable to or only slightly higher than that of universal control Lipofectamine2000*. However, the fact that some transfection capacity has been observed, as well as the promising cell viabilities measured for TMAC4/DOPE-pDNA lipoplexes, provide a pathway for improving this new kind of nonviral gene vector involving macrocyclic polycationic lipid-based molecules.

CONCLUSIONS

The biophysical and biochemical characterization of TMAC4/DOPE-pDNA lipoplexes confirms that the calixarene-based polycationic lipidic vector TMAC4 is able to compact and transfect the pEGFP-C3 plasmid in a safe way. The zeta potential study of TMAC4/DOPE-ctDNA shows that TMAC4 has 100% of its nominal charge available (q^+_{CxCL} = +4), and pDNA presents an effective negative charge that is only 10% of its nominal one, all this data being confirmed by gel electrophoresis experiments. PALS studies indicate the presence of three populations of nanoaggregates in TMAC4/DOPE lipid mixtures without pDNA with sizes of approximately 100, 17, and 6 nm compatible with liposomes, oblate micelles, and spherical micelles, respectively. The presence of liposomes and oblate micelles was confirmed by cryo-TEM studies, as well. However, TMAC4/DOPE-pDNA lipoplexes are organized in multilamellar L_α nanostructures at all CxCL molar fractions as confirmed by SAXS experiments. Moreover, cryo-TEM micrographs show two types of multilamellar aggregation patterns: cluster-type (CT) at low and moderate CxCL molar fractions (α = 0.2 and 0.5) and fingerprint-type (FP) present only at low CxCL molar fractions (α = 0.2). AFM results for TMAC4/DOPE-pDNA samples at α = 0.2 also evidence that the presence of pDNA makes the lipid bilayer more deformable, thus enhancing the capability to penetrate cells. Finally, the best transfection performances of these TMAC4/DOPE-pDNA lipoplexes, with regard to TE and cellular viability levels, have been seen at low CxCL molar fractions (α = 0.2) and a moderate-to-high effective charge ratio ρ_{eff} = 20. The coexistence of two lamellar phases has once again been suggested as a synergistic factor that enhances TE performance at low α composition.

AUTHOR INFORMATION

Corresponding Author

*Fax: +34913944135. E-mail: junquera@quim.ucm.es.

Funding

MICINN of Spain, Project CTQ2012-30821.

Notes

The authors declare no competing financial interest.

ACKNOWLEDGMENTS

The authors thank MICINN of Spain. SAXS experiments were performed at NCD11 beamline at ALBA Synchrotron Light Facility with the collaboration of the ALBA staff. The authors also thank C. Aicart-Ramos for performing the amplification of plasmid DNA at the Departamento de Bioquímica y Biología Molecular I (UCM, Spain), J. Fernández-Rosas for the synthesis of TMAC4 at the Departamento de Química Física (CIQUS, USC, Spain), and P. Castro-Hartmann, Servei de Microscopia of UAB (Spain), for cryo-TEM experiments.

REFERENCES

(1) Thomas, Clare E.; E, A.; K, M. A. Progress and Problems with the Use of Viral Vectors for Gene Therapy. *Nat. Rev. Genet.* **2003**, *4*, 346–358.

(2) Junquera, E.; Aicart, E. Cationic Lipids as Transfecting Agents of DNA in Gene Therapy. *Curr. Topics Med. Chem.* **2014**, *14* (5), 649–663.

(3) Ibraheem, D.; Elaissari, A.; Fessi, H. Gene Therapy and DNA Delivery Systems. *Int. J. Pharm.* **2014**, *459* (1–2), 70–83.

DOI: 10.1021/acsami.5b03231
ACS Appl. Mater. Interfaces 2015, 7, 14404–14414

(4) Tros de Ilarduya, C.; Garcia, L.; Duzgunes, N. Liposomes and Lipopolymeric Carriers for Gene Delivery. *J. Microencapulation* **2010**, *27* (7), 602−608.
(5) Somia, N.; Verma, I. M. Gene Therapy: Trials and Tribulations. *Nat. Rev. Genet* **2000**, *1* (2), 91−99.
(6) Verma, I. M.; Somia, N. Gene Therapy - Promises, Problems and Prospects. *Nature* **1997**, *389*, 239−242.
(7) Felgner, P. L. Nonviral Strategies for Gene Therapy. *Sci. Am.* **1997**, *276*, 102−106.
(8) Pozzi, D.; Marchini, C.; Cardarelli, F.; Rossetta, A.; Colapicchioni, V.; Amici, A.; Montani, M.; Motta, S.; Brocca, P.; Cantu, L.; Caracciolo, G. Mechanistic Understanding of Gene Delivery Mediated by Highly Efficient Multicomponent Envelope-Type Nanoparticle Systems. *Mol. Pharmaceutics* **2013**, *10* (12), 4654−4665.
(9) Sharma, V. D.; Ilies, M. A. Heterocyclic Cationic Gemini Surfactants: A Comparative Overview of Their Synthesis, Self-Assembling, Physicochemical, and Biological Properties. *Med. Res. Rev.* **2014**, *34* (1), 1−44.
(10) Zhi, D.; Zhang, S.; Cui, S.; Zhao, Y.; Wang, Y.; Zhao, D. The Headgroup Evolution of Cationic Lipids for Gene Delivery. *Bioconjugate Chem.* **2013**, *24* (4), 487−519.
(11) Caracciolo, G.; Amenitsch, H. Cationic Liposome/DNA Complexes: From Structure to Interactions with Cellular Membranes. *Eur. Biophys. J.* **2012**, *41* (10), 815−829.
(12) Estevez-Torres, A.; Baigl, D. DNA Compaction: Fundamentals and Applications. *Soft Matter* **2011**, *7* (15), 6746−6756.
(13) de Ilarduya, C. T.; Sun, Y.; Duezguenes, N. Gene Delivery by Lipoplexes and Polyplexes. *Eur. J. Pharm. Sci.* **2010**, *40* (3), 159−170.
(14) Bhattacharya, S.; Bajaj, A. Advances in Gene Delivery through Molecular Design of Cationic Lipids. *Chem. Commun.* **2009**, *31*, 4632−4656.
(15) Pozzi, D.; Caracciolo, G.; Caminiti, R.; De Sanctis, S. C.; Amenitsch, H.; Marchini, C.; Montani, M.; Amici, A. Toward the Rational Design of Lipid Gene Vectors: Shape Coupling between Lipoplex and Anionic Cellular Lipids Controls the Phase Evolution of Lipoplexes and the Efficiency of DNA Release. *ACS Appl. Mater. Interfaces* **2009**, *1* (10), 2237−2249.
(16) Al-Dosari, M. S.; Gao, X. Nonviral Gene Delivery: Principle, Limitations, and Recent Progress. *AAPS J.* **2009**, *11* (4), 671−681.
(17) Wettig, S. D.; Verrall, R. E.; Foldvari, M. Gemini Surfactants: A New Family of Building Blocks for Non-Viral Gene Delivery Systems. *Curr. Gene Ther.* **2008**, *8* (1), 9−23.
(18) Karmali, P. P.; Chaudhuri, A. Cationic Liposomes as Non-Viral Carriers of Gene Medicines: Resolved Issues, Open Questions, and Future Promises. *Med. Res. Rev.* **2007**, *27* (5), 696−722.
(19) Wasungu, L.; Hoekstra, D. Cationic Lipids, Lipoplexes and Intracellular Delivery of Genes. *J. Controlled Release* **2006**, *116* (2), 255−264.
(20) Ewert, K.; Slack, N. L.; Ahmad, A.; Evans, H. M.; Lin, A. J.; Samuel, C. E.; Safinya, C. R. Cationic Lipid-DNA Complexes for Gene Therapy: Understanding the Relationship between Complex Structure and Gene Delivery Pathways at the Molecular Level. *Curr. Med. Chem.* **2004**, *11* (2), 133−149.
(21) Kirby, A. J.; Camilleri, P.; Engberts, J.; Feiters, M. C.; Nolte, R. J. M.; Soderman, O.; Bergsma, M.; Bell, P. C.; Fielden, M. L.; Rodriguez, C. L. G.; Guedat, P.; Kremer, A.; McGregor, C.; Perrin, C.; Ronsin, G.; van Eijk, M. C. P. Gemini Surfactants: New Synthetic Vectors for Gene Transfection. *Angew. Chem., Int. Ed.* **2003**, *42* (17), 1448−1457.
(22) Templeton, N. S. Cationic Liposome-Mediated Gene Delivery in Vivo. *Biosci. Rep.* **2002**, *22* (2), 283−295.
(23) Barran-Berdon, A. L.; Misra, S. K.; Datta, S.; Muñoz-Ubeda, M.; Kondaiah, P.; Junquera, E.; Bhattacharya, S.; Aicart, E. Cationic Gemini Lipids Containing Polyoxyethylene Spacers as Improved Transfecting Agents of Plasmid DNA in Cancer Cells. *J. Mater. Chem. B* **2014**, *2* (29), 4640−4652.
(24) Ortiz Mellet, C.; Benito, J. M.; Garcia Fernandez, J. M. Preorganized, Macromolecular, Gene-Delivery Systems. *Chem.−Eur. J.* **2010**, *16* (23), 6728−6742.
(25) Bagnacani, V.; Sansone, F.; Donofrio, G.; Baldini, L.; Casnati, A.; Ungaro, R. Macrocyclic Nonviral Vectors: High Cell Transfection Efficiency and Low Toxicity in a Lower Rim Guanidinium Calix[4]-Arene. *Org. Lett.* **2008**, *10* (18), 3953−3956.
(26) Lai, W. F. Cyclodextrins in Non-Viral Gene Delivery. *Biomaterials* **2014**, *35* (1), 401−411.
(27) Nakamura, E.; Isobe, H.; Tomita, N.; Sawamura, M.; Jinno, S.; Okayama, H. Functionalized Fullerene as an Artificial Vector for Transfection. *Angew. Chem., Int. Ed.* **2000**, *39* (23), 4254−4257.
(28) Nierengarten, I.; Nothisen, M.; Sigwalt, D.; Biellmann, T.; Holler, M.; Remy, J.-S.; Nierengarten, J.-F. Polycationic Pillar[5]Arene Derivatives: Interaction with DNA and Biological Applications. *Chem.−Eur. J.* **2013**, *19* (51), 17552−17558.
(29) Bagnacani, V.; Franceschi, V.; Bassi, M.; Lomazzi, M.; Donofrio, G.; Sansone, F.; Casnati, A.; Ungaro, R. Arginine Clustering on Calix[4]Arene Macrocycles for Improved Cell Penetration and DNA Delivery. *Nat. Commun.* **2013**, *4*, 1721.
(30) Aoyama, Y. Macrocyclic Glycoclusters: From Amphiphiles through Nanoparticles to Glycoviruses. *Chem.−Eur. J.* **2004**, *10* (3), 588−593.
(31) Aoyama, Y.; Kanamori, T.; Nakai, T.; Sasaki, T.; Horiuchi, S.; Sando, S.; Niidome, T. Artificial Viruses and Their Application to Gene Delivery. Size-Controlled Gene Coating with Glycocluster Nanoparticles. *J. Am. Chem. Soc.* **2003**, *125* (12), 3455−3457.
(32) Rodik, R. V.; Anthony, A.-S.; Kalchenko, V. I.; Mely, Y.; Klymchenko, A. S. Cationic Amphiphilic Calixarenes to Compact DNA into Small Nanoparticles for Gene Delivery. *New J. Chem.* **2015**, *39* (3), 1654−1664.
(33) Rodik, R.; Klymchenko, A.; Mely, Y.; Kalchenko, V. Calixarenes and Related Macrocycles as Gene Delivery Vehicles. *J. Inclusion Phenom. Macrocyclic Chem.* **2014**, 1−12.
(34) McMahon, G.; O'Malley, S.; Nolan, K.; Diamond, D. Important Calixarene Derivatives − Their Synthesis and Applications. *ARKIVOC (Gainesville, FL, U.S.)* **2003**, *2003*, 23−31.
(35) Bize, C.; Garrigues, J. C.; Blanzat, M.; Rico-Lattes, I.; Bistri, O.; Colasson, B.; Reinaud, O. Spontaneous Formation of Vesicles in a Catanionic Association Involving a Head and Tail Functionalized Amino-Calix[6]Arene. *Chem. Commun.* **2010**, *46* (4), 586−588.
(36) Dudic, M.; Colombo, A.; Sansone, F.; Casnati, A.; Donofrio, G.; Ungaro, R. A General Synthesis of Water Soluble Upper Rim Calix[*N*]Arene Guanidinium Derivatives Which Bind to Plasmid DNA. *Tetrahedron* **2004**, *60* (50), 11613−11618.
(37) Hayashida, O.; Mizuki, K.; Akagi, K.; Matsuo, A.; Kanamori, T.; Nakai, T.; Sando, S.; Aoyama, Y. Macrocyclic Glycoclusters. Self-Aggregation and Phosphate-Induced Agglutination Behaviors of Calix[4]Resorcarene-Based Quadruple-Chain Amphiphiles with a Huge Oligosaccharide Pool. *J. Am. Chem. Soc.* **2003**, *125* (2), 594−601.
(38) Rodik, R. V.; Klymchenko, A. S.; Jain, N.; Miroshnichenko, S. I.; Richert, L.; Kalchenko, V. I.; Mely, Y. Virus-Sized DNA Nanoparticles for Gene Delivery Based on Micelles of Cationic Calixarenes. *Chem.−Eur. J.* **2011**, *17* (20), 5526−5538.
(39) Sansone, F.; Dudič, M.; Donofrio, G.; Rivetti, C.; Baldini, L.; Casnati, A.; Cellai, S.; Ungaro, R. DNA Condensation and Cell Transfection Properties of Guanidinium Calixarenes: Dependence on Macrocycle Lipophilicity, Size, and Conformation. *J. Am. Chem. Soc.* **2006**, *128* (45), 14528−14536.
(40) Nimse, S. B.; Kim, T. Biological Applications of Functionalized Calixarenes. *Chem. Soc. Rev.* **2013**, *42* (1), 366−386.
(41) Kumar, K.; Barran-Berdon, A. L.; Datta, S.; Munoz-Ubeda, M.; Aicart-Ramos, C.; Kondaiah, P.; Junquera, E.; Bhattacharya, S.; Aicart, E. A Delocalizable Cationic Headgroup Together with an Oligo-Oxyethylene Spacer in Gemini Cationic Lipids Improves Their Biological Activity as Vectors of Plasmid DNA. *J. Mater. Chem. B* **2015**, *3* (8), 1495−1506.
(42) Muñoz-Ubeda, M.; Misra, S. K.; Barran-Berdon, A. L.; Data, S.; Aicart-Ramos, C.; Castro-Hartmann, P.; Kondaiah, P.; Junquera, E.; Bhattacharya, S.; Aicart, E. How Does the Spacer Length of Cationic Gemini Lipids Influence the Lipoplex Formation with Plasmid DNA?

DOI: 10.1021/acsami.5b03231
ACS Appl. Mater. Interfaces 2015, 7, 14404−14414

Physicochemical and Biochemical Characterizations and Their Relevance in Gene Therapy. *Biomacromolecules* **2012**, *13*, 3926−3937.
(43) Muñoz-Ubeda, M.; Misra, S. K.; Barran-Berdon, A. L.; Aicart-Ramos, C.; Sierra, M. B.; Biswas, J.; Kondaiah, P.; Junquera, E.; Bhattacharya, S.; Aicart, E. Why Is Less Cationic Lipid Required to Prepare Lipoplexes from Plasmid DNA Than Linear DNA in Gene Therapy? *J. Am. Chem. Soc.* **2011**, *133*, 18014−18017.
(44) Misra, S. K.; Muñoz-Ubeda, M.; Datta, S.; Barran-Berdon, A. L.; Aicart-Ramos, C.; Castro-Hartmann, P.; Kondaiah, P.; Junquera, E.; Bhattacharya, S.; Aicart, E. Effects of a Delocalizable Cation on the Headgroup of Gemini Lipids on the Lipoplex-Type Nanoaggregates Directly Formed from Plasmid DNA. *Biomacromolecules* **2013**, *14* (11), 3951−3963.
(45) Strobel, M.; Kita-Tokarczyk, K.; Taubert, A.; Vebert, C.; Heiney, P. A.; Chami, M.; Meier, W. Self-Assembly of Amphiphilic Calix[4]Arenes in Aqueous Solution. *Adv. Funct. Mater.* **2006**, *16* (2), 252−259.
(46) Düker, M. H.; Gómez, R.; Vande Velde, C. M. L.; Azov, V. A. Upper Rim Tetrathiafulvalene-Bridged Calix[4]Arenes. *Tetrahedron Lett.* **2011**, *52* (22), 2881−2884.
(47) Rodriguez-Pulido, A.; Aicart, E.; Llorca, O.; Junquera, E. Compaction Process of Calf Thymus DNA by Mixed Cationic-Zwitterionic Liposomes: A Physicochemical Study. *J. Phys. Chem. B* **2008**, *112* (7), 2187−2197.
(48) Dubochet, J.; Adrian, M.; Chang, J. J.; Homo, J. C.; Lepault, J.; McDowall, A. W.; Schultz, P. Cryo-Electron Microscopy of Vitrified Specimens. *Q. Rev. Biophys.* **1988**, *21*, 129−228.
(49) Bednar, J.; Woodcock, C. L. In *Chromatin*; Academic Press Inc.: San Diego, 1999; Vol. *304*, p 191−213.
(50) Dubochet, J.; Zuber, B.; Eltsov, M.; Bouchet-Marquis, C.; Al-Amoudi, A.; Livolant, F. How to "Read" a Vitreous Section. *Methods Cell Biol.* **2007**, *79*, 385−406.
(51) Muñoz-Ubeda, M.; Rodriguez-Pulido, A.; Nogales, A.; Llorca, O.; Quesada-Perez, M.; Martin-Molina, A.; Aicart, E.; Junquera, E. Gene Vectors Based on Doepc/Dope Mixed Cationic Liposomes: A Physicochemical Study. *Soft Matter* **2011**, *7*, 5991−6004.
(52) Hansen, M. B.; Nielsen, S. E.; Berg, K. Re-Examination and Further Development of a Precise and Rapid Dye Method for Measuring Cell-Growth Cell Kill. *J. Immunol. Methods* **1989**, *119*, 203−210.
(53) Bajaj, A.; Kondiah, P.; Bhattacharya, S. Design, Synthesis, and in Vitro Gene Delivery Efficacies of Novel Cholesterol-Based Gemini Cationic Lipids and Their Serum Compatibility: A Structure-Activity Investigation. *J. Med. Chem.* **2007**, *50* (10), 2432−2442.
(54) Barran-Berdon, A. L.; Muñoz-Ubeda, M.; Aicart-Ramos, C.; Perez, L.; Infante, M. R.; Castro-Hartmann, P.; Martin-Molina, A.; Aicart, E.; Junquera, E. Ribbon-Type and Cluster-Type Lipoplexes Constituted by a Chiral Lysine Based Cationic Gemini Lipid and Plasmid DNA. *Soft Matter* **2012**, *8* (28), 7368−7380.
(55) Battersby, B. J.; Grimm, R.; Huebner, S.; Cevc, G. Evidence for Three-Dimensional Interlayer Correlations in Cationic Lipid-DNA Complexes as Observed by Cryo-Electron Microscopy. *Biochim. Biophys. Acta* **1998**, *1372*, 379−383.
(56) Huebner, S.; Battersby, B. J.; Grimm, R.; Cevc, G. Lipid-DNA Complex Formation: Reorganization and Rupture of Lipid Vesicles in the Presence of DNA as Observed by Cryoelectron Microscopy. *Biophys. J.* **1999**, *76* (6), 3158−3166.
(57) Tarahovsky, Y. S.; Rakhmanova, V. A.; Epand, R. M.; MacDonald, R. C. High Temperature Stabilization of DNA in Complexes with Cationic Lipids. *Biophys. J.* **2002**, *82*, 264−273.
(58) Rosa, M.; Moran, M. D.; Miguel, M. D.; Lindman, B. The Association of DNA and Stable Catanionic Amino Acid-Based Vesicles. *Colloids Surf., A* **2007**, *301* (1−3), 361−375.
(59) Rosa, M.; Miguel, M. D.; Lindman, B. DNA Encapsulation by Biocompatible Catanionic Vesicles. *J. Colloid Interface Sci.* **2007**, *312* (1), 87−97.
(60) Muñoz-Ubeda, M.; Rodriguez-Pulido, A.; Nogales, A.; Martin-Molina, A.; Aicart, E.; Junquera, E. Effect of Lipid Composition on the Structure and Theoretical Phase Diagrams of Dc-Chol/Dope-DNA Lipoplexes. *Biomacromolecules* **2010**, *11* (12), 3332−3340.
(61) Schneider, J.; Dufrene, Y. F.; Barger, W. R., Jr.; Lee, G. U. Atomic Force Microscope Image Contrast Mechanisms on Supported Lipid Bilayers. *Biophys. J.* **2000**, *79* (2), 1107−1118.

DOI: 10.1021/acsami.5b03231
ACS Appl. Mater. Interfaces 2015, 7, 14404−14414